Low-pressure CVD of (Tix,W1-x)Ny from WF6, TiCl4 and NH3

Downloaded from: https://research.chalmers.se, 2026-04-06 05:36 UTC

Citation for the original published paper (version of record):
Gerdin Hulkko, J., Qiu, R., Bäcke, O. et al (2022). Low-pressure CVD of (Tix,W1-x)Ny from WF6, TiCl4 and NH3. Surface and Coatings Technology, 438.
http://dx.doi.org/10.1016/j.surfcoat.2022.128394

N.B. When citing this work, cite the original published paper.

research.chalmers.se offers the possibility of retrieving research publications produced at Chalmers University of Technology. It covers all kind of research output: articles, dissertations, conference papers, reports etc. since 2004. research.chalmers.se is administrated and maintained by Chalmers Library

(article starts on next page)

Surface & Coatings Technology 438 (2022) 128394

Contents lists available at ScienceDirect

Surface & Coatings Technology

journal homepage: www.elsevier.com/locate/surfcoat

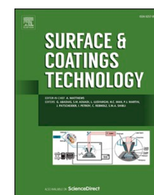

Low-pressure CVD of $(Ti_x,W_{1-x})N_y$ from WF_6, $TiCl_4$ and NH_3

Johan G. Hulkko [a,*], Ren Qiu [b], Olof Bäcke [b], Axel Forslund [c,d], Mats Halvarsson [b], Henrik Larsson [c], Mats Boman [a]

[a] Uppsala University, Department of Chemistry–Ångström Laboratory, 75120 Uppsala, Sweden
[b] Chalmers University of Technology, Department of Physics, 41296 Gothenburg, Sweden
[c] Royal Institute of Technology (KTH), Unit of Structures, 12679 Hägersten, Sweden
[d] Institute for Materials Science, University of Stuttgart, 70569 Stuttgart, Germany

ARTICLE INFO

Keywords:
CVD
Ternary ceramic
Nitride
TiWN
Hard materials
ERDA

ABSTRACT

In this work chemical vapour deposited (CVD) coatings of $(Ti_x,W_{1-x})N_y$ from $TiCl_4$, WF_6, NH_3 and Ar were investigated. This coating material has previously been deposited using other vacuum techniques but no publication has so far demonstrated CVD of $(Ti_x,W_{1-x})N_y$. The studied $(Ti_x,W_{1-x})N_y$ coatings had a metallic molar ratio (Ti:W) close to 2:1 and 1:1, and were slightly over-stoichiometric with regard to N. The coatings appeared homogeneous and crystallised in a rock salt structure on an α-Al_2O_3 substrate. The cell parameter varied between 4.16 and 4.23 Å as a function of the deposition conditions, ranging from a pure TiN_x to a pure WN_x coating. The texture in the normal direction was ⟨100⟩ for the TiN_x and $(Ti_x,W_{1-x})N_y$ coatings and ⟨111⟩ for WN_x. Electron backscattered diffraction (EBSD) results showed that a strong correlation to the substrate existed but random in-plane orientation was also present. The microstructure showed columnar grains with well defined facets growing. Adding a mixture of $TiCl_4$ and WF_6 to produce $(Ti_x,W_{1-x})N_y$ did increase the grain size significantly when compared to the case when only one metal precursor was present. The down-stream thickness profile, using only WF_6 and NH_3, displayed mass transport control behaviour, with the coating thickness converging to zero within the deposition zone. Using only $TiCl_4$ on the other hand showed a uniform deposition profile, the signs of a surface kinetics controlled process.

1. Introduction

In the field of protective coatings there are a lot of materials in use today. Commonly, such coatings are synthesised directly on the surface that should be protected, using for instance wet chemical or vapour deposition methods. These coatings are typically in the range of a few microns thick but due to their toughness and hardness, this is in most cases all that is needed to produce a sufficient protection for the underlying material. One commonly used material is TiN_x, having a high hardness and also an appealing golden colour. Another material is WN_x, which is also hard. These two nitride materials are refractory and their properties have been used in applications as gate materials [1,2] and diffusion barriers in microelectronic devices [3,4]. Their structures are both of the B1-type (rock salt) and together they are thermodynamically driven to form a ternary solid solution, $(Ti_x,W_{1-x})N_y$. This phase is, as could be expected, also a hard material and has some promising properties. When it comes to very hard materials, there is a trade-off between hardness and toughness. Generally, one needs to sacrifice one for the other. Forming a harder material will often make it more brittle; while making it ductile turns it softer. It has been found that in some cases the combination of hardness and ductility can indeed be improved for certain materials by adding a third element. One famous case being TiAlN [5], that experiences spinodal decomposition when subjected to heat or high workloads i.e. during cutting operations. The single phase decomposes into two phases and the material undergoes several hardening processes leading to an extended coating life time. Some prior work investigating ternary nitrides in general, $(A_x,B_{1-x})N_y$, has been reviewed by Kindlund et al. (A, B = Ti, Zr, V, Hf, Cr, Mo, W, Ta, Nb) [6] where the complex theory for hardness and toughness is described as difficult and still not well understood. The currently common way to categorise physical properties of cubic B1 transition metal nitrides is through the valence electron concentration (VEC). VEC refers to the filling of d-electrons in shear resistive (e_g) and shear sensitive (t_{2g}) states. As the VEC is increased, the shear resistive states begin to become

Abbreviations: ERDA, Elastic Recoil Detection Analysis; CVD, Chemical Vapour Deposition.

* Corresponding author.
E-mail address: johan.gerdin@kemi.uu.se (J.G. Hulkko).

https://doi.org/10.1016/j.surfcoat.2022.128394
Received 6 February 2022; Received in revised form 3 March 2022; Accepted 22 March 2022
Available online 1 April 2022
0257-8972/© 2022 The Authors. Published by Elsevier B.V. This is an open access article under the CC BY license (http://creativecommons.org/licenses/by/4.0/).

occupied. A maximum filling of these states is reported at 8.4 electrons per formula unit (e./f.u) at which point the shear sensitive states begins to fill. Now hardness becomes reduced but ductility increases. The maximum toughness lies in the range of 9.5–10.5 e./f.u. In the work by Glechner [7], this was shown by alloying a hafnium carbide with nitrogen thus raising the VEC. A maximum for the hardness was found for a VEC slightly beneath 10 e./f.u. The measured fracture toughness was increased from 1.89 to 2.33 MPa × $m^{½}$. The binary nitrides of Ti and W are reported to have VEC levels of 10 and 11 e./f.u, respectively. Thus, ternary nitrides of Ti and W are excellent candidate materials for maximising both hardness and toughness. The field of ternary nitrides is dominated by physically vapour deposited (PVD) thin films, where several papers have been published on the synthesis of $(Ti_x,W_{1-x})N_y$ [8,9]. One possible explanation for this domination is that PVD is a great method for screening. The target source materials used can be made to be unevenly distributed across the substrate surface in a controlled manner. This allows for elemental composition gradients to be deposited in one experiment which saves time and money. The CVD method is quite different from PVD and offers several advantages. CVD coatings can be uniform in thickness, even on complex substrate geometries, and can be very dense compared to other techniques due to the high deposition temperature. One disadvantage is that the process of CVD is more complex and can require complex precursors in order to get a material with a satisfactory stoichiometry or texture. The complexity arises from the vast variable space and interaction between temperature, total pressure, partial pressures of reactive gases and products as well as the profile of the gas flow. One publication regarding CVD-$(Ti_x,W_{1-x})C_y$ using $W(CO)_6$ can be found at the time of writing [10]. No prior work regarding CVD of $(Ti_x,W_{1-x})N_y$ coatings appears to exist in the literature.

Both the low pressure (LP) CVD-TiN_x and LPCVD-WN_x processes are achievable in the 1 Torr range. This was the starting point for this study and the process was regarded as a co-deposition process of the two individual materials. The partial reaction orders in the $TiCl_4$–NH_3 [11,12] system in regard to p_{NH3} is ~1.3 while for p_{TiCl4} it is −0.5. In the WF_6–NH_3 system the partial reaction orders is closer to 1/2 for p_{NH3} and 1/6 for p_{WF6} [13]. Knowing that the reaction rate of WF_6 is fast it is expected that the coatings might become W-rich and for balance, the kinetics of both processes were considered. The $TiCl_4$:WF_6 molar ratio in the gas phase is therefore kept high. Both processes are more limited by the ammonia rather than the metal halide. Increasing p_{NH3} would overall benefit the deposition of Ti, while increasing p_{TiCl4} would suppress it. WF_6 will etch Ti to form TiF_4(g). Mixed halides, in the form of MX_zY_{6-z}, can form (e.g. WF_5Cl) according to earlier work using WF_6 and $TiCl_4$. The work by Fraser et al. [14] suggest these compounds are very unstable and will most likely decompose quickly as the reactor temperature is increased. The final consideration was that WF_6 is reacting rapidly and can be depleted quickly. In such a case, if the sample is positioned far from the gas inlet, the p_{WF6} deviate from the known input values. In this case, it is difficult to make good conclusions without having knowledge about the local partial pressure, which could be measured with, for instance, a mass spectrometer.

The aim for this paper is to elucidate on the possibility of using CVD to deposit a ternary $(Ti_x,W_{1-x})N_y$ from WF_6, $TiCl_4$ and NH_3 precursors. The scope is to theoretically calculate the possible phases from the currently available data. Samples are deposited by varying the partial pressures of these precursor gases while keeping a constant deposition temperature and a low constant pressure. Using Time of Flight Elastic Recoil Detection Analysis (TOF-ERDA), X-ray fluorescence (XRF) and X-ray diffraction (XRD), the elemental and phase contents are evaluated for some selected coatings. Electron microscopy and EBSD is employed to gain insight to the microstructure of the coatings.

2. Methods

2.1. Thermodynamic calculations

A thermodynamic calculation is made for an isolated system and takes in the deposition temperature, total pressure, precursor amounts as well as material data from a material database. The output is a set of phases and their corresponding amounts for which the energy of the system is minimised. For the thermodynamic calculations the Thermo-Calc software package was used with the TCFE9 database. The phase labelled (Ti,W)N is a face centred cubic phase with N on the interstitial sublattice, the phase labelled W here is a body centred cubic phase and h-WN is a hexagonal nitride phase. Separate calculations were performed to investigate the thermodynamically stable phases in equilibrium when: (1) only solid phases are allowed; and (2) when formation of N_2-gas is permitted. For the Ti-W-N system, the results presented here are based on interpolation between binary data, as no ternary Ti-W-N data has been assessed previously.

2.2. LPCVD synthesis

The synthesis of $(Ti_x,W_{1-x})N_y$ was performed in a horizontal tube reactor. The reactor has been described elsewhere [15]. Two substrate materials were used: (000l) oriented α-Al_2O_3 substrates from MTI Corporation were used as received without any additional cleaning. This substrate material is relatively inert, provides a well-defined surface and is easily characterised by diffraction. The second substrate material was silica in the form of 22 cm long bars. These bars were used in two experiments to investigate the varying coating thickness along the deposition zone. These were rinsed with ethanol, blown dry with Ar and placed to cover a downstream distance of 1–45 cm from the gas inlet. The α-alumina substrates were positioned 5 cm downstream from the gas inlet on top of the silica bars. To reduce the variable space, the sample positions were fixed and the deposition temperature (789 K), total pressure (1 Torr) and total volumetric flow rate (350 SCCM) were kept constant. Then only four variables remain which are the individual partial pressures of gases. These partial pressures are set by the mass flow by which the gases are introduced to the reactor. The partial pressure of metal halide was kept fixed at 0.0429 Torr. The partial pressures of $TiCl_4$ (99.9% Acros Organics), WF_6 (5.5 N Matheson Gas) and NH_3 (3.6 N Aga gas AB) were then varied according to Table I. The $TiCl_4$ was kept in a 150 ml 316 L stainless steel canister heated to 57.5°. The flow of $TiCl_4$ was regulated by an MKS1152C-unit operated at 60 °C. The flow of $TiCl_4$ was calibrated by taking the mass difference of the canister after a known length of time using a few constant set-point values. The flows of WF_6, NH_3 and Ar were regulated using MKS GM50A-units using the factory calibration. The substrate surface was treated with NH_3 for 5 min prior to and after the deposition process, while the reactor was at thermal equilibrium. The pre-deposition

Table I
Summary of the deposition conditions used. The temperature was fixed at 789 K at a total pressure of 1 Torr. The linear flow velocity across the substrate surface was approximately 3 m/s using a total volumetric flow rate of 350 SCCM.

Sample	p_{WF6} [Torr]	p_{TiCl4} [Torr]	p_{NH3} [Torr]	p_{Ar} [Torr]
A	0	0.0429	0.2571	0.7000
B	0.0014	0.0414	0.2571	0.7000
C	0.0029	0.0400	0.2571	0.7000
D	0.0429	0	0.2571	0.7000
E	0	0.0429	0.2143	0.7429
F	0.0057	0.0371	0.2143	0.7429
G	0.0029	0.0400	0.0857	0.8714
H	0.0057	0.0371	0.0857	0.8714
I	0.0014	0.0414	0.0429	0.9143
J	0.0057	0.0371	0.0429	0.9143
K	0.0429	0	0.0429	0.9143

treatment was conducted to stabilise the gas phase with regard to the decomposition of NH_3 and to saturate the substrate surface in order to mitigate possible etching. The post-deposition step was performed in order to further remove unreacted halide within the reactor and coating.

2.3. Elemental composition

Some selected coatings were further analysed by TOF-ERDA. This method is based on the physical collision of an incident ion and the atomic nuclei of sample material. Depending on the mass difference of the atomic nuclei, the sample atoms will be forward scattered. The displaced sample atoms are detected and both their speeds and energies are measured. This then allows for mass and probe depth determination. By employing heavier incident ions, lighter sample atoms, such as C, N, O and F, will be forward scattered to a greater degree. This makes TOF-ERDA very sensitive to low-Z elements and ideal for determining the content of C and N in carbides and nitrides.

The TOF-ERDA experiments were performed with a 36 MeV $^{127}I^{+8}$ beam incident at 67.5° with the surface normal and recoil angle of 45°. The TOF-ERDA detector consists of a time-of-flight telescope followed by a gas ionisation chamber, so that both energy and time-of-flight of recoiled particles were recorded. The compositions were obtained from depth profiles with the software Potku were the compositions converged.

The elemental compositions of the deposited coatings were also analysed using XRF. This method relies on X-ray excitations of the atoms within the sample. As the atoms are de-excited through fluorescence, the yield of emitted photons is being counted. This fluorescence yield, at a specific characteristic transition of one type of atom, can then be correlated to the respective number of atoms of that kind. XRF is limited to heavier elements due to the limited number of electrons able to interact in low-Z elements such as nitrogen. As such, quantitative analysis of $(Ti_x,W_{1-x})N_y$ coatings is effectively limited to the Ti:W molar ratio. On the positive side, the analysis is fast and non-destructive, saving time for planning and execution of subsequent experiments.

XRF was performed using an Epsilon 3 instrument from PANalytical. The fluorescence yield was measured using a 1 mm thick Cu-mask on Teflon with a Ø 4 mm hole to keep the illuminated area constant. For titanium analysis, the Ti$K\alpha_1$ was used. For tungsten analysis, the W$L\beta_{1,2}$ peaks were chosen since the W$L\alpha_{1,2}$ contributions overlap the Cu$K\alpha_{1,2}$ and Cu$K\beta_1$ signals from the Cu-mask. The relative concentrations of the elements were calculated by integrating the selected Ti$K\alpha_1$ and W$L\beta_{1,2}$ peaks.

2.4. Phase composition

Phase composition was analysed using XRD. θ/2θ diffraction data in the out-of-plane direction was recorded in the span of 2θ = 30–150°. XRD was performed on the samples using a D5000-system from Siemens with a CuKα source (1.5418 Å). θ/2θ-data were collected using a standard Bragg-Brentano geometry with motorised divergence and anti-scatter slits at 0.15° and 1°, respectively, and a 0.2 mm receiving slit. A curved graphite monochromator was equipped with a 1 mm detector slit. The fitting of the diffraction peaks was done in the Topas-software by Bruker. Le Bail-phases were used, keeping the peak positions fixed but allowing for instance the intensity and cell parameter to be fitted to the data.

2.5. Electron microscopy

The surface morphology of the coatings was studied using a Zeiss 1530 instrument equipped with a Schottky field emission gun (FEG) source. In-lens secondary electron images were acquired using an acceleration voltage of 2 kV and a working distance of ~4.7 mm.

Cross sections of the coatings were polished using an FEI Versa 3D focused ion beam – SEM (FIB-SEM) system with the Ga ion beam being parallel to the normal direction of the substrate (the stage was tilted by 52°). The cross sections were imaged with the electron beam in the FIB-SEM system while the stage was titled by 52° (the angle between the electron beam and the substrate). Electron backscattered diffraction (EBSD) was measured on the unpolished surfaces of the $(Ti_x,W_{1-x})N_y$ coatings using a Tescan GAIA FIB-SEM system equipped with an Oxford NanoNordlys detector, and the EBSD data was analysed using Oxford HKL software.

3. Result and discussion

3.1. Thermodynamic calculations

A ternary isotherm at 789 K is shown in Fig. 1a. If the gas phase (N_2) is included, thereby effectively limiting the nitrogen activity to one relative gas at 1 bar pressure and ambient temperature, the cubic W_2N decomposes into W and h-WN or into W and gas. Fig. 1b shows the same isotherm but excluding the gas phase from the calculation. The β-W_2N and h-WN_x then appears in the W-N binary, with low Ti solubility in equilibrium with the B1-TiN_x with some solubility of W (labelled (Ti,W)

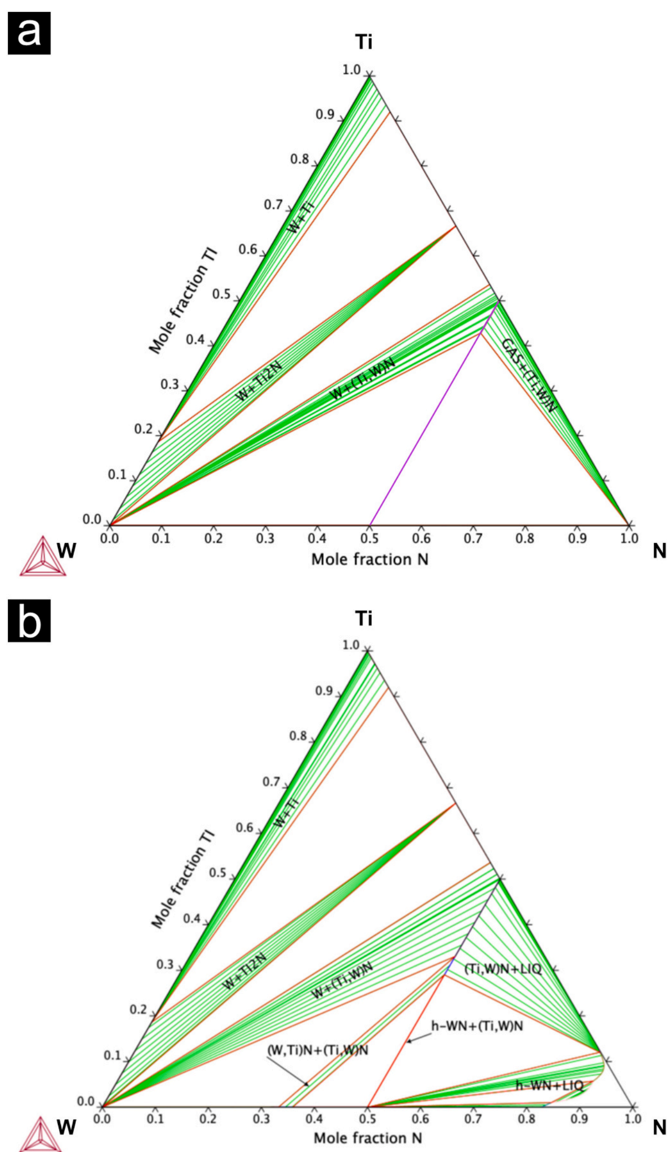

Fig. 1. a) Isothermal section including N_2-gas at 789 K and 1 Torr. b) Isothermal section excluding N_2-gas at 789 K and 1 Torr.

N). In Fig. 2 an isopleth at 0.5 mol fraction N is show as function of mole fraction Ti and temperature. At high Ti content, W dissolves in the $(Ti_x, W_{1-x})N_y$ phase, while if the W content is larger than 0.67–0.61 mol fraction it will precipitate as hexagonal WN below 789 K. At higher temperatures on the other hand, this hexagonal nitride decomposes into bcc W metal and N_2 gas. The pseudo-binary diagram in Fig. 2 corresponds to the isoplethal section with a composition marked by the purple line in the isotherm in Fig. 1a. As can be seen from there, at 789 K, any addition of N would go to the gas phase, while any depletion of N would result in a sub-stoichiometric $(Ti_x,W_{1-x})N_y$ phase with no W on the metallic sublattice, i.e. in TiN_{1-x}.

In the TCFE9 database, the cubic WN and W_2N have low solubilities of Ti. On the other hand, the TiN phase shows a larger solubility of W. As stated, an assessment of the ternary W-Ti-N system is lacking, but the W_2N phase with some contents of Ti have shown to stay in solid solution under annealing up to 1100 K [16]. Another study [17] reports formation of a secondary B1-TiN phase at TiN contents between 10–20%, but a stable solution below those contents. Thus, one could probably expect a slightly larger solubility of TiN_x in the cubic W-nitride than predicted in the ternary isotherm presented here, in Figs. 1–2.

3.2. Elemental composition

The elemental composition analysis was performed with TOF-ERDA. It was observed that the nitrogen content generally settled around 50 at. %. The metal molar ratio was heavily skewed in favour of tungsten deposition. At the highest investigated p_{NH3}, samples A–D, a ratio of $TiCl_4$:WF_6 = 13:2 in the gas phase resulted in a coating content of close to $(Ti_{0.2}W_{0.2})N_{0.5}$. All samples displayed some halide contamination in TOF-ERDA of ~10 at.%. This was also examined and confirmed briefly using Energy dispersive spectroscopy (EDS) on the coating cross sections. The results for samples A–D are plotted in Fig. 3. Also worth remarking is that a yellow precipice was deposited downstream outside the furnace when $TiCl_4$ was present. This was assumed to be an adduct between $TiCl_4$ and NH_3 as has been reported on previously [18].

It was found that the Ti and W coating concentrations does not follow the partial pressure linearly. While there may be several reasons for this, one of the simplest explanations is that the amount of chlorine is in one unit of $TiCl_4$ is not equal to the amount of fluorine in one unit of WF_6. As p_{TiCl4} is increased and p_{WF6} is reduced, the amount of NH_3 per halogen (F or Cl) is increased. There is virtually more ammonia to $TiCl_4$ when compared to WF_6 and this will, according to the kinetics of the individual reactions, benefit the deposition of TiN_x on the surface more than the deposition of WN_x. Another reason is the reactivity and kinetics which was investigated using XRF at the deposition conditions for samples A (TiN_x-process) and D (WN_x-process). The silica bar sample holder was cut and the relative fluorescence yield at different positions within the reactor were compared. It was observed that the relative Ti-content in the TiN_x-process within the first 40 cm of the reactor was constant as is expected for process governed by surface kinetics. In the WN_x-process the relative W-content diminished during the first 30 cm, at which point the gas phase appeared fully depleted and resulted in no W-deposition. The integrated fluorescence yield is provided in Fig. 4.

For the WN_x coating, it was not possible to make measurements further upstream due to the stress levels within the coating. This region suffered from severe cracking and delamination on the silica bar. It was thus not possible to determine if a region where a relatively stable concentration of tungsten was deposited which would indicate that the process in the upstream region was governed by surface kinetics. The fast decline in coating thickness in the down-stream direction suggest that mass transport control is in effect.

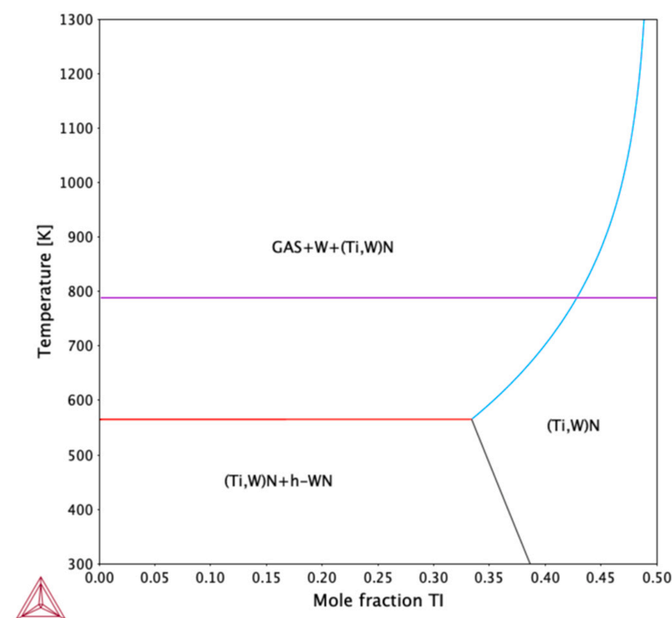

Fig. 2. Pseudo-binary isopleth including N_2-gas at 0.5 mol fraction N at 789 K (Purple line) and 1 Torr. (For interpretation of the references to colour in this figure legend, the reader is referred to the web version of this article.)

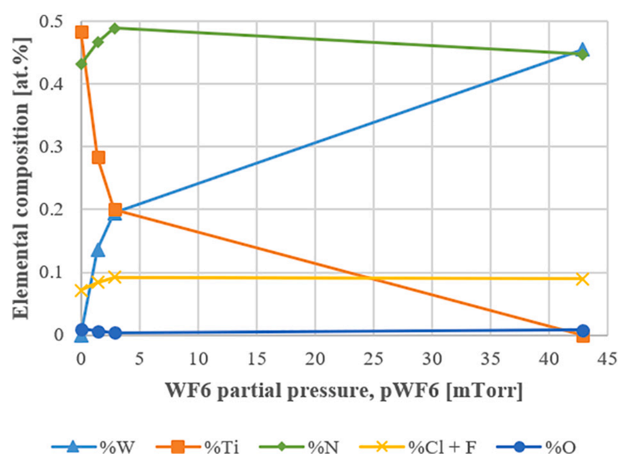

Fig. 3. The coating composition evaluated by ERDA as a function of p_{WF6}. Total metal halide partial pressure of p_{MX} = 0.0429 (MX = $TiCl_4$ + WF_6) and p_{NH3} = 0.2571, T = 789 K, P = 1 Torr and p_{NH3} = 260 mTorr corresponding to samples A–D.

3.3. Phase composition

XRD was employed to evaluate the phase content and to estimate the cell parameter of the deposited phase. Apart from the two substrate material peaks (α-Al_2O_3 (0006) and (000 12)), the samples in general

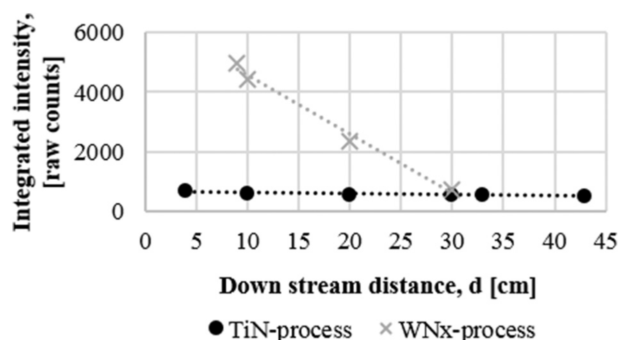

Fig. 4. The relative metal content for the sample processes A (TiN_x) and D (WN_x) across the deposition zone.

displayed only one major phase, cubic TiN_x or cubic β-W_2N. The exceptions being samples B, which displayed peaks that could be assigned to two phases, TiN and β-W_2N. The phases could be fitted using either the TiN (PDF 038-1420) or β-W2N (PDF 025-1257) patterns by allowing the cell parameter to be changed. The acquired out-of-plane θ/2θ data of samples A–D are plotted in Fig. 5. The values of the cell parameter reduced gradually from 4.23 Å (ref = 4.24 Å) to 4.16 Å (ref = 4.13 Å) as p_{WF6} was increased and p_{TiCl4} was reduced within the gas mixture. The cell parameter also followed p_{NH3} but to a lesser extent. The cell parameter, plotted as a function of the W/(Ti + W) atomic fraction acquired by XRF, can be seen in Fig. 6. The metal composition acquired by XRF deviates from the values retrieved by TOF-ERDA due to the lower sensitivity of the measurement. It, however, provides for a quick and non-destructive acquisition of data which allowed a larger pool of samples to be analysed. It does not provide information regarding the concentration of nitrogen.

When comparing the TOF-ERDA data and XRD phase content to the thermodynamic calculations, it is seen that these CVD depositions have not reached thermodynamic equilibrium. This is expected as CVD is a steady state process with new precursor added and by-products expelled from the system. Limits in the diffusion rate may also hinder the material from reaching equilibrium thus rendering the material meta stable. The elemental composition is close to N at.% = 50 % which is represented by the pseudo-binary isopleth presented in Fig. 2 previously. At a deposition temperature of 789 K in the same figure, calculations suggest that a concentration of Ti at.% < ~ 43% would yield a mix of W and $(Ti_x,W_{1-x})N_y$ within the coating. Samples B and C showed no indication of a W phase present in XRD even though the respective concentrations were closer to 30 and 20 at.% respectively.

The trend in the cell parameter, as seen in Fig. 6, does span within the two expected boundary values, a_{TiNx} = 4.24 Å and a_{WNx} = 4.16 Å. The expected value of WN_x here is higher than the PDF reference since a previous study of WN_x coatings of the same phase produced in this apparatus [13] did come to the same value. Those coatings were considered free of contamination as measured by TOF-ERDA. One method for roughly estimating the cell parameter within a solid solution is the use of Vegard's rule. This empirical relationship, defined in terms for this system, is: $a_{(Tix,W1-x)Ny} = x * a_{WNx} + (1 - x) * a_{TiNx}$. Comparing the plotted values to the values given by Vegard's rule shows a decent agreement but deviate slightly from it. The samples on the W-rich end are underestimated with the opposite being true on the Ti-rich end. The reason for this discrepancy can partly be attributed to error in the XRF measurement and partly to the unknown quantity of N present in these coatings. For instance, a higher content of N occupying vacancies and/or tetrahedral-/octahedral holes would expand the cell. Internal stresses in

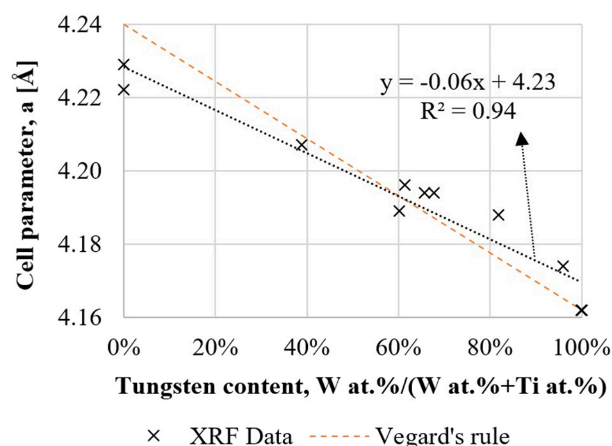

Fig. 6. The cell parameter as a function of the tungsten fraction of the metal content for samples A–K. Samples at 0 or 100 % are deposited using either only $TiCl_4$ or WF_6.

the coating could affect the value of the cell parameter too. The thickness of the closely investigated samples A–D is seen in Fig. 7 in the next section. There it is seen that the thickness of the TiN_x (sample A) is rather thin, 600 nm. A thicker sample, being more bulk-like, is more relaxed and may not express the condition of stresses at, for instance, the substrate interface. Thinner samples may for this reason also deviate from the expected cell parameter value.

3.4. Microstructure

The morphologies and microstructures of some selected samples, A–D were investigated by SEM. Micrographs of the samples A–D are provided in Fig. 7. It can be seen that samples A (TiN_x), B and C ($(Ti_x,W_{1-x})N_y$) exhibit growth into wedge shaped grains that displays well defined top facets. Sample D (WN_x) appears very featureless in the cross-section and it displays a top surface with less defined surface features which is confirmed by the WN_x-Pt interface in the polished cross-section.

It can be concluded that homogenous $(Ti_x,W_{1-x})N_y$ coatings have been deposited. The microstructure is wedge shaped which is common to a deposition process in growth mode. There is some contrast to the cross-sections of A–C but that is due to channelling contrast and not inhomogeneity in the atomic distribution. The featureless appearance of the WN_x film is attributed to nano-crystallinity.

EBSD was performed on the unpolished top surface of the samples to

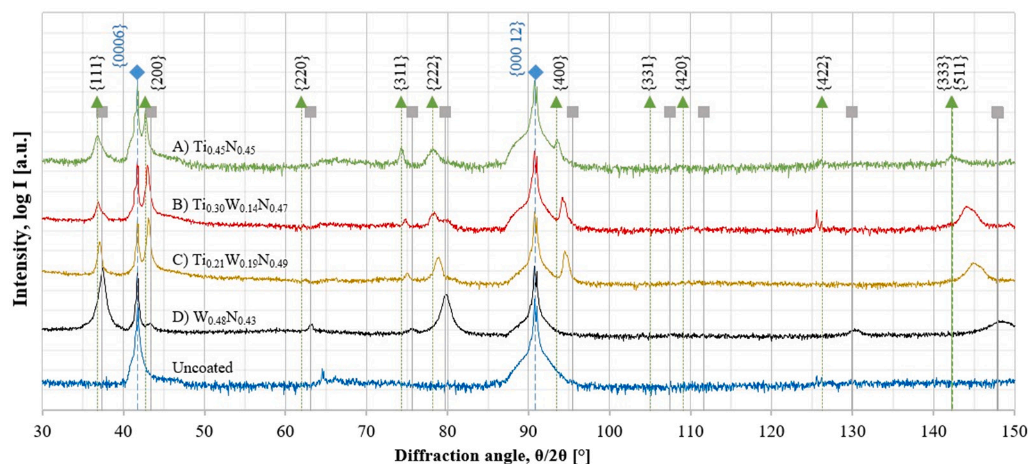

Fig. 5. θ/2θ out-of-plane diffraction data of samples A–D deposited at 789 K and at 1 Torr using at a constant p_{NH3}. Elemental composition by TOF-ERDA given out of 1 with unassigned remainder being contaminant (mostly F and/or Cl).

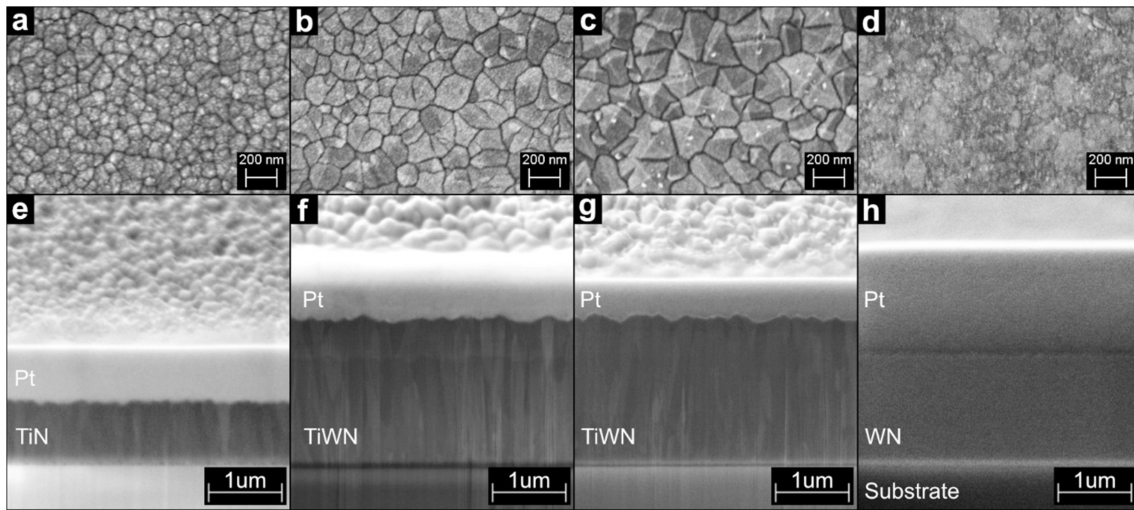

Fig. 7. (a–d) Unpolished planar view and (e–h) cross section view with Pt on top for (a, e) sample A (TiN_x), (b, f) sample B ($(Ti_x,W_{1-x})N_y$), (c, g) sample C ($(Ti_x,W_{1-x})N_y$) and (d, h) sample D (WN_x).

provide texture information in the form of pole figures. All four of the investigated samples A–D showed clear textures which is displayed in Fig. 8 by the high intensities at the centres of the pole figures. Samples A–C showed an ⟨100⟩ alignment with the coating normal and sample D displayed a ⟨111⟩ orientation. This is supported by the XRD data shown earlier in Fig. 5.

The three samples (A-C) with ⟨100⟩ textures all exhibit a dotted ring at the periphery of the pole figures, i.e. 90° away from the coating normal, that can be explained by crystal symmetries and coating nucleation. The samples with a ⟨100⟩ texture will exhibit a 4-fold symmetry around the coating normal in the {100} pole figures (Fig. 8a (top)). Given the α-Al_2O_3 substrate surface 3-fold symmetry, three different, but energetically equivalent, nucleation and growth orientations are expected, giving a total of $3 \times 4 = 12$ intensities near the periphery in the {100} pole figures. These different nucleation orientations are represented by coloured squares in Fig. 8a–c. As for sample D with a ⟨111⟩ out-of-plane orientation, this alignment is expected to fit well with the substrate, however looking at the {111} pole figure (Fig. 8d) there are three additional poles present. For a single crystal oriented along ⟨111⟩, the pole figure would yield four poles, $(11\bar{1})$, $(1\bar{1}1)$, $(\bar{1}11)$, separated by 120°, and (111) located in the centre. If the stacking order is reversed by nucleation of a twinned crystallite, those poles are no longer visible. Instead the $(\bar{1}\bar{1}1)$, $(\bar{1}1\bar{1})$, $(1\bar{1}\bar{1})$ poles are seen, also separated by 120° but offset by 60° to their mirror parts. This is illustrated by the coloured triangles in Fig. 8b. The $(\bar{1}\bar{1}\bar{1})$ pole overlaps the (111) pole and does not yield an additional pole in the figure. The present of twinned grains explain the poles observed here by EBSD.

4. Conclusions

We have successfully produced crystalline $(Ti_x,W_{1-x})N_y$ coatings from a WF_6, $TiCl_4$ and NH_3 reaction gas mixture using CVD. The coatings displayed a cubic phase with a cell parameter in between TiN and β-W_2N (see Figs. 5–7). It was shown that the element composition could be varied by adjusting the gas phase composition over the substrate surface (see Fig. 4). By adjusting the gas phase composition toward more $TiCl_4$, to compensate for the higher reaction rate of WF_6, a coating having equal amounts of Ti and W was achieved.

The deposition conditions were not optimised in regard to phase purity and texture control. The introduction of additional NH_3 or H_2 to

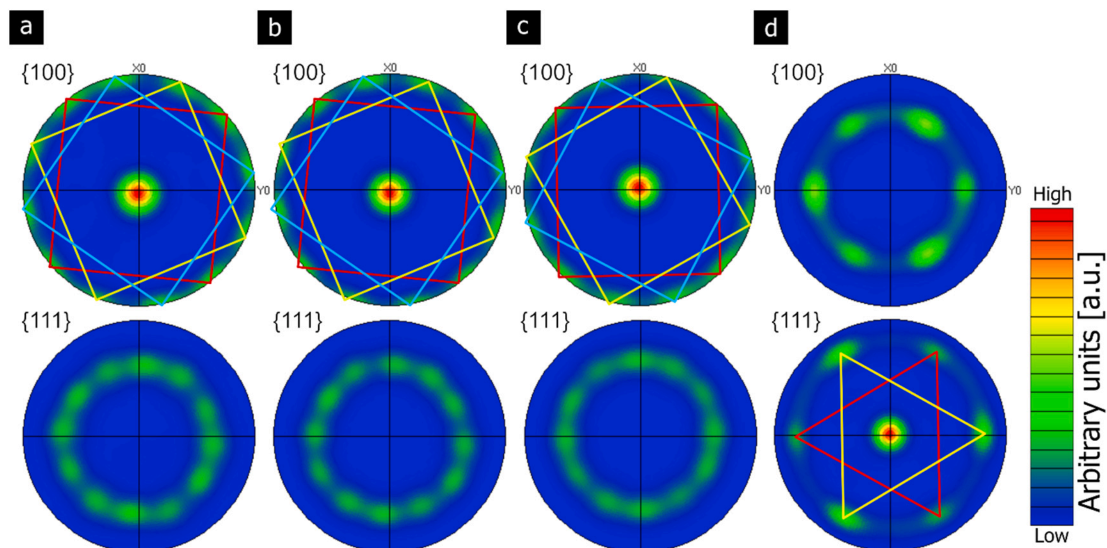

Fig. 8. {100} and {111} pole figures of (a) sample A (TiN_x), (b) sample B ($(Ti_x,W_{1-x})N_y$), (c) sample C ($(Ti_x,W_{1-x})N_y$) and (d) sample D (WN_x).

the reaction gas mixture may reduce the halide (F and Cl) contamination which were between 5 and 10%. Future experiments may take into consideration the depletion of WF_6 that affects the length of the deposition zone and coating compositions. The grains in the ternary coatings were wedge shaped and, when compared to the binary TiN and β-W_2N, they were significantly larger (see Fig. 7). The texture of the $(Ti_x,W_{1-x})N_y$ samples were ⟨100⟩ and is was shown that there is an epitaxial relationship to the substrate (see Fig. 8). There was some tendency toward random in-plane orientation that is likely related to a loss of coherency as the sample grows thicker and the internal stresses level out.

CRediT authorship contribution statement

Johan G. Hulkko: Conceptualization, Methodology, Software, Investigation, Formal analysis, Data curation, Validation, Visualization, Writing – original draft, Writing – review & editing. **Ren Qiu:** Investigation, Formal analysis, Visualization, Writing – review & editing. **Olof Bäcke:** Investigation, Formal analysis, Visualization, Writing – review & editing. **Axel Forslund:** Investigation, Formal analysis, Visualization, Writing – original draft, Writing – review & editing. **Mats Halvarsson:** Supervision, Funding acquisition, Writing – review & editing. **Henrik Larsson:** Supervision, Writing – review & editing. **Mats Boman:** Supervision, Funding acquisition, Writing – review & editing.

Declaration of competing interest

The authors declare that they have no known competing financial interests or personal relationships that could have appeared to influence the work reported in this paper.

Acknowledgements

The work and the CVD 2.0-project was supported by the Swedish Foundation for Strategic Research via SSF contract RMA15-0048; by Sandvik AB, Sweden; the Inorganic Chemistry programme at Chemistry Ångström, Uppsala university, Sweden.

The EBSD and coating cross sectional imaging were carried out at the Chalmers Materials Analysis Lab (CMAL).

The XRF measurements provided by Katalin Böőr at the Inorganic Chemistry programme at Chemistry Ångström, Uppsala university are greatly appreciated.

References

[1] S. Youn, K. Roh, S. Yang, Y. Roh, K.-S. Kim, Y.-C. Jang, N.-E. Lee, Investigation of the W-TiN metal gate for metal–oxide–semiconductor devices, J. Vac. Sci. Technol. A 19 (2001) 1591–1594, https://doi.org/10.1116/1.1345913.
[2] Wang, Cyclical Deposition of Tungsten Nitride For Metal Oxide Gate Electrode, Dec. 21, 2004. US Patent: US 6,833,161 B2.
[3] M. Mühlbacher, F. Mendez-Martin, B. Sartory, N. Schalk, J. Keckes, J. Lu, L. Hultman, C. Mitterer, Copper diffusion into single-crystalline TiN studied by transmission electron microscopy and atom probe tomography, Thin Solid Films 574 (2015) 103–109, https://doi.org/10.1016/j.tsf.2014.11.084.
[4] N. Gonohe, Tungsten nitride deposition by thermal chemical vapor deposition as barrier metal for cu interconnect, Mater. Trans. 43 (7) (2002) 1585–1592, https://doi.org/10.2320/matertrans.43.1585.
[5] R. Qiu, A. Forslund, O. Bäcke, A.H.S. Iyer, M. Sattari, W. Janssen, T. Manns, J. Kümmel, A. Ruban, D. Stiens, H.-O. Andrén, M. Halvarsson, Effects of gas flow on detailed microstructure inhomogeneities in LPCVD TiAlN nanolamella coatings, Materialia 9 (2020), https://doi.org/10.1016/j.mtla.2019.100546.
[6] H. Kindlund, D.G. Sangiovanni, I. Petrov, J.E. Greene, L. Hultman, A review of the intrinsic ductility and toughness of hard transition-metal nitride alloy thin films, Thin Solid Films 688 (2019), https://doi.org/10.1016/j.tsf.2019.137479.
[7] T. Glechner, S. Lang, R. Hahn, M. Alfreider, V. Moraes, D. Primetzhofer, J. Ramm, S. Kolozsvári, D. Kiener, H. Riedl, Correlation between fracture characteristics and valence electron concentration of sputtered hf-C-N based thin films, Surf. Coat. Technol. 399 (2020), https://doi.org/10.1016/j.surfcoat.2020.126212.
[8] L.R. Shaginyan, M. Misina, J. Zemek, J. Musil, F. Regent, V.F. Britun, Composition, structure, microhardness and residual stress of W-Ti–N films deposited by reactive magnetron sputtering, Thin Solid Films 408 (2002) 136–147, https://doi.org/10.1016/S0040-6090(02)00091-3.
[9] F. Tian, J. D'Arcy-Gall, T.-Y. Lee, M. Sardela, D. Gall, I. Petrov, J.E. Greene, Epitaxial Ti1-xWxN alloys grown on MgO(001) by ultrahigh vacuum reactive magnetron sputtering: electronic properties and long-range cation ordering, J. Vac. Sci. Technol. A 21 (2003) 140–146, https://doi.org/10.1116/1.1525818.
[10] H.X. Ji, C.C. Amato-Wierda, Chemical vapor deposition of ti-W-C thin films, Surf. Coat. Technol. 148 (2–3) (2001) 262–267, https://doi.org/10.1016/S0257-8972(01)01342-1.
[11] M.J. Buiting, A.F. Otterloo, A.H. Montree, Kinetical aspects of the LPCVD of titanium nitride from titanium tetrachloride and ammonia, J. Electrochem. Soc. 138 (1991) 500–505, https://doi.org/10.1149/1.2085618.
[12] N. Ramanuja, R.A. Levy, S.N. Dharmadhikari, E. Ramos, C.W. Pearce, S. C. Menasian, P.C. Schamberger, C.C. Collins, Synthesis and characterization of low pressure chemically vapor deposited titanium nitride films using TiCl4 and NH3, Mater. Lett. 57 (2) (2002) 261–269, https://doi.org/10.1016/S0167-577X(02)00776-0.
[13] J.G. Hulkko, K. Böőr, R. Qiu, O. Bäcke, M. Boman, M. Halvarsson, E. Lindahl, Kinetics of the low-pressure chemical vapor deposited tungsten nitride process using tungsten hexafluoride and ammonia precursors, J. Vac. Sci. Technol. A 39 (2021), https://doi.org/10.1116/6.0001093.
[14] G.W. Fraser, C.J.W. Gibbs, R.D. Peacock, Tungsten chloride fluorides: the preparation of cis- and trans-tungsten dichloride tetrafluoride and its decomposition into other tungsten fluorides, J. Chem. Soc. A (1970) 1708–1711, https://doi.org/10.1039/J19700001708.
[15] J.G. Hulkko, Muspel and Surtr: CVD system and control program for WF6 chemistry, Thesis, Uppsala university, 2019, http://urn.kb.se/resolve?urn=urn:nbn:se:uu:diva-380973.
[16] C.-S. Lee, E.-Y. Chang, L. Chang, C.-Y. Fang, Y.-L. Huang, J.-S. Huang, Study of titanium tungsten nitride and tungsten nitride Schottky contacts on n-GaN, Jpn. J. Appl. Phys. 42 (2003), 7R, https://doi.org/10.1143/JJAP.42.4193.
[17] H. Ju, N. Ding, J. Xu, L. Yu, I. Asempah, J. Xu, G. Yi, B. Ma, Crystal structure and the improvement of the mechanical and tribological properties of tungsten nitride films by addition of titanium, Surf. Coat. Technol. 345 (2018) 132–139, https://doi.org/10.1016/j.surfcoat.2018.04.021.
[18] S.R. Kurtz, R.G. Gordon, Chemical vapor deposition of titanium nitride at low temperatures, Thin Solid Films 140 (2) (1986) 277–290, https://doi.org/10.1016/0040-6090(86)90271-3.